Geomechanics and Engineering, *Vol. 21, No. 2 (2020) 179-186*
DOI: https://doi.org/10.12989/gae.2020.21.2.179

Development of seismic fragility curves for high-speed railway system using earthquake case histories

Seunghoon Yang[1a], Dongyoup Kwak*[1] and Tadahiro Kishida[2b]

[1]*Department of Civil and Environmental Engineering, Hanyang University, ERICA, 55 Hanyangdaehak-ro, Sangnok-gu, Ansan-si, Gyeonggi-do 15588, Republic of Korea*
[2]*Department of Civil Infrastructure and Environmental Engineering, Khalifa University of Science and Technology, Abu Dhabi, U.A.E.*

(Received December 4, 2019, Revised January 19, 2020, Accepted March 3, 2020)

Abstract. Investigating damage potential of the railway infrastructure requires either large amount of case histories or in-depth numerical analyses, or both for which large amounts of effort and time are necessary to accomplish thoroughly. Rather than performing comprehensive studies for each damage case, in this study we collect and analyze a case history of the high-speed railway system damaged by the 2004 M6.6 Niigata Chuetsu earthquake for the development of the seismic fragility curve. The development processes are: 1) slice the railway system as 200 m segments and assigned damage levels and intensity measures (IMs) to each segment; 2) calculate probability of damage for a given IM; 3) estimate fragility curves using the maximum likelihood estimation regression method. Among IMs considered for fragility curves, spectral acceleration at 3 second period has the most prediction power for the probability of damage occurrence. Also, viaduct-type structure provides less scattered probability data points resulting in the best-fitted fragility curve, but for the tunnel-type structure data are poorly scattered for which fragility curve fitted is not meaningful. For validation purpose fragility curves developed are applied to the 2016 M7.0 Kumamoto earthquake case history by which another high-speed railway system was damaged. The number of actual damaged segments by the 2016 event is 25, and the number of equivalent damaged segments predicted using fragility curve is 22.21. Both numbers are very similar indicating that the developed fragility curve fits well to the Kumamoto region. Comparing with railway fragility curves from HAZUS, we found that HAZUS fragility curves are more conservative.

Keywords: high-speed railway; fragility curve; 2004 Niigata Chuetsu earthquake; 2016 Kumamoto earthquake; Shinkansen; damage level

1. Introduction

High-speed railway system is an effective and fast transportation system connecting cities. To maintain its high speed, the railway tends to be built straight. Hence, the railway system is composed of composite infrastructures including tunnel, bridge, and viaducts which are vulnerable to seismic motions.

Seismic vulnerability of tunnel, bridge, viaduct, or roadbed through which high-speed trains pass have been key research subjects for railway seismic reliability study (Argyroudis and Pitilakis 2012, Argyroudis and Kaynia 2015, Balkaya and Kalkan 2004, da Porto *et al.* 2016, Li *et al.* 2017, Liu *et al.* 2015, Lu *et al.* 2019, Shao *et al.* 2014, Yilmaz *et al.* 2019). Analyzing damage potential of each infrastructure needs either large amounts of data sets, in-depth numerical analyses, or both, which require multiple research efforts to accomplish thoroughly.

Seismic reliability is often expressed as fragility curves –the probability exceeding a certain damage level (*DL*) conditioning on certain intensity measures (*IMs*). HAZUS, FEMA's methodology estimating potential losses from natural disasters, provides earthquake loss estimation model for railway transportation system (Kircher *et al.* 2014). Fragility curves for track and roadbeds, bridges, tunnels, and facilities are shown in the HAZUS technical manual (FEMA 2014). Kim *et al.* (2014) analyzed seismic fragility of tunnels that are belong to the Korean high-speed railway system analytically and compared fragility curves from HAZUS.

In this study, for evaluation of seismic reliability of high-speed railway system, we perform case history analysis. The advantage of this analysis is that it uses real damage observations and measured *IMs* so that it can be used for validation of the fragility curves developed analytically (Kwak *et al.* 2016). Targeting case histories in this study are the Shinkansen Joetsu Line (SJL) damaged by the 2004 **M**6.6 Niigata Chuetsu earthquake and the Shinkansen Kyushu Line (SKL) damaged by the 2016 **M**7.0 Kumamoto earthquake. At each event, a train was derailed due to the ground shaking, and numerous damage were occurred along the railway. The major damage by the 2004 event is observed from Echigo-Yuzawa to Niigata station where the length is approximately 118 km, and observed from Shinminamata to Shinomuta station where the length is approximately 113 km at the 2016 event. For the 2004 event we could gather locations of railway damage, but for

*Corresponding author, Ph.D., Assistant Professor
E-mail: dkwak@hanyang.ac.kr
[a]M.Sc. Student
[b]Ph.D., Assistant Professor

http://www.techno-press.org/?journal=gae&subpage=7 ISSN: 2005-307X (Print), 2092-6219 (Online)

the 2016 event the damage location is very uncertain. Therefore, we use the 2004 event case history for fragility model development and use the 2016 event case history for model validation.

In the previous study (Yang and Kwak 2019) we collected damage states of the railway system damaged by the 2004 event from the damage observation report (Ogura 2006) and defined damage levels following the damage states from the HAZUS earthquake loss estimation model for a railway infrastructure (FEMA 2014). Five ground motion *IMs* (PGA, PGV, $SA_{T0.3}$, $SA_{T1.0}$, $SA_{T3.0}$) were assessed from the USGS ShakeMap program (USGS 2019a). With the seismic demands and number of damaged segments, seismic fragility curves were evaluated depending on each IM statistically. From the results, Yang and Kwak (2019) suggest that the fragility curve with 3 second spectral acceleration ($SA_{T3.0}$) performs the best (i.e., predicts the damage with the least uncertainty). However, in the previous study the fragility curve was suggested for the entire railway system without dividing into sub-structure type. In this study, we evaluate fragility curves for each structure type (i.e., tunnel and viaduct) and validate the model by comparing with the total number of damaged segments at another system by the 2016 event.

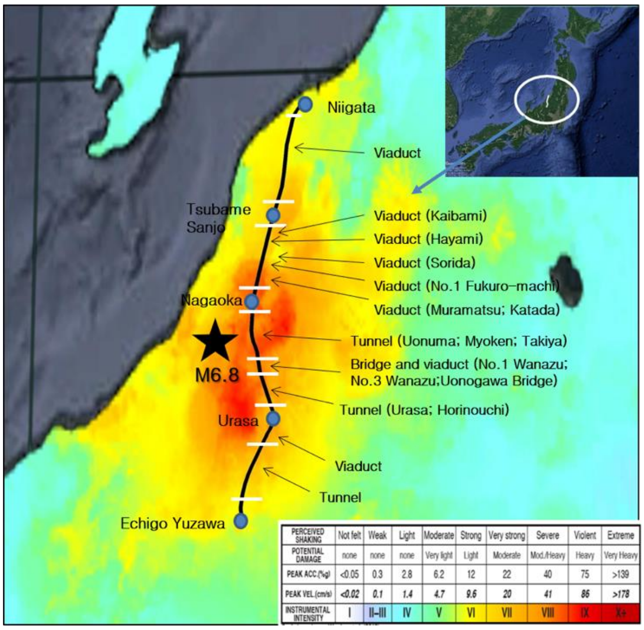

Fig. 1 Location of SJL, and seismic intensity contour map (USGS 2019a)

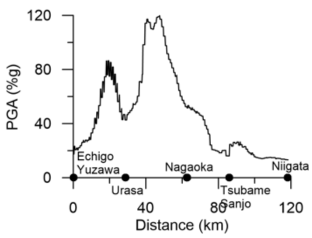

(a) Peak ground acceleration (%g)

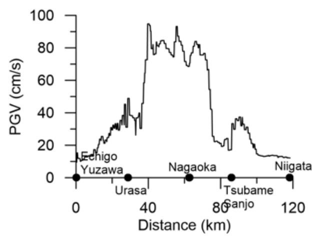

(b) Peak ground velocity (cm/s)

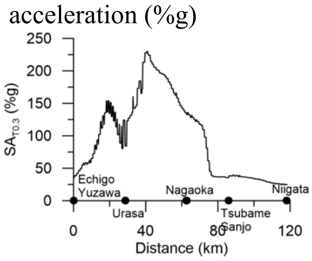

(c) Spectral acceleration at T=0.3 sec (%g)

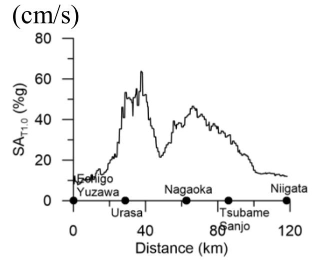

(d) Spectral acceleration at T=1.0 sec (%g)

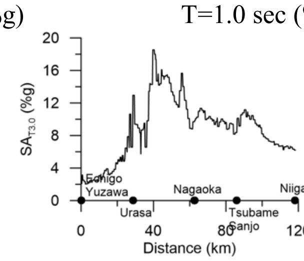

(e) Spectral acceleration at T=3.0 sec (%g)

Fig. 2 Intensity measures by the 2004 Niigata event. Distance metric is measured from Echigo-Yuzawa station along the SJL

2. Case histories of high-speed railway system damaged by earthquakes

This section summarizes damage states of high-speed railway systems and seismic demands for two case histories.

*2.1 2004 **M**6.6 Niigata Chuetsu earthquake*

2.1.1 Target system and earthquake demand

The 2004 **M**6.6 Niigata Chuetsu earthquake occurred inland in Niigata region, Japan, where the Shinkansen Joetsu Line (SJL) locates near the epicenter. Due to seismic excitation, various levels of damage were occurred on the SJL between Echigo-Yuzawa and Niigata stations. Location of the SJL, railway structure type, and shaking intensity are shown in Fig. 1. Looking satellite imageries and road-view along the SJL, we could group structure types as three: 1) station, 2) viaduct or bridge, and 3) tunnel. The total length is 70.4 km for viaduct or bridge and 46.4 km for tunnel. We collected various *IMs* including short to long period components of ground motions (i.e., PGA, PGV, $SA_{T0.3}$, $SA_{T1.0}$, and $SA_{T3.0}$) from USGS ShakeMap (USGS 2019a) along the railway, which are plotted in Fig. 2.

2.1.2 Damage distribution

From the damage observation report (Ogura 2006), we classified damage descriptions and assigned damage levels as described in Table 1 (Yang and Kwak 2019). To prepare statistical analysis described in the subsequent section, we sliced the target SJL system into 200 m segments. The unit length of 200 m is selected because the general minimum length of the Shinkansen train set is approximately 200 m (one set is composed of 8-12 cars, and each car length is approximately 25 m). As a result, the target system is sliced into 592 segments. Each segment was categorized as aforementioned three structure types (station, viaduct or bridge, and tunnel), and *DL* was assigned based on the damage description.

Table 1 Damage levels assigned to each damage description for the SJL case history

DL	Damage state	Target structure type	Damage description
1	Slight	Station	- Catenary poles tilted - Snow-melting station damaged
		Viaduct	
2	Minor	Tunnel	- Fallen concrete
		Viaduct	- 1-4 columns damaged
3	Moderate	Tunnel	- Composite damage (fallen concrete, slab track deformation, crack in central passageway)
		Viaduct	- > 4 columns damaged
4	Extensive	Viaduct	- Ground subsidence - Rail deformation

To evaluate fragility curve, it is important to know the exact location of damage to incorporate *IM* with *DL*. However, damage locations are not fully described in the damage observation report so that we needed to interpret and approximated the locations. For example, a catenary pole damage case is written in the report as “44 catenary poles tilted between Echigo-Yuzawa and Urasa stations.” Unfortunately, we do not know where those 44 tilted poles were located exactly at this time. Hence, we equally distributed the damage states to all segments between Echigo-Yuzawa and Urasa stations for this case. There are 143 segments between these two stations. From satellite imagery, we figured out that there are 10 poles in one 200 m length segment. Thus, 44 poles would locate within 4.4 segments as the least. Since the total number of segments is 143, we assign 3% weight to each segment, which is the potential of pole damage. Note that 100% weight indicates that at least one damage feature is observed within a segment. In this way, we could distribute each damage states to the whole railway system if locations are not specified. If a damage state is specified within a segment (e.g., damage at two columns in Uonogawa Bridge), full weight is assigned to the segment.

2.2 2016 Kumamoto Earthquake sequence

2.2.1 Target system and earthquake demand

The 2016 Kumamoto earthquakes have two devastating events: one is the **M**6.2 foreshock, and the other is the **M**7.0 mainshock. Both events damaged a high-speed railway system, Shinkansen Kyushu Line (SKL). Similar to the Niigata case history, we gathered damage information from a damage observation report, assessed seismic demands from USGS ShakeMap, and specified SKL structure type along the railway. Fig. 3 shows location of SKL with seismic intensity map from the **M**7.0 mainshock, and Fig. 4 shows *IMs* along the SKL between Shinminamata and Shinomuta stations where damage occurred by both events.
It is an opportunity that we could collect two case histories (foreshock and mainshock) for the same system, but in the same time it is difficult to analyse because we do not know which damage was occurred by which event. Moreover, damage locations are uncertain comparing to the Niigata case which hinder our interpretation. Therefore, we do not use this data set for fragility curve development but use for model validation.

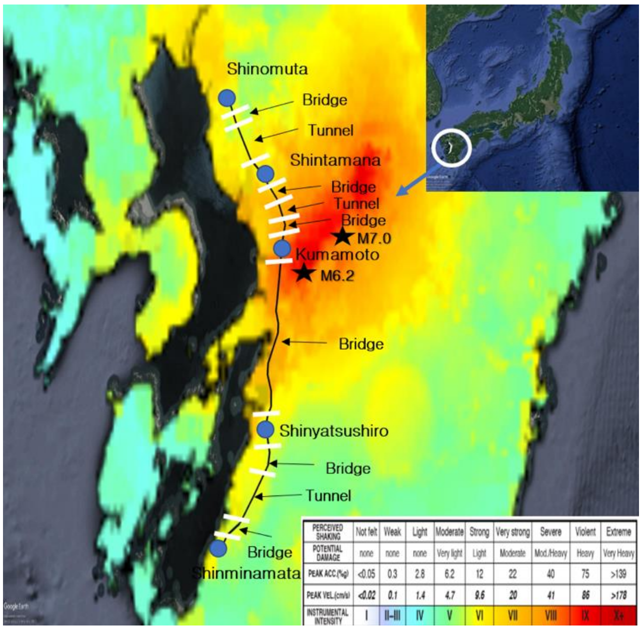

Fig. 3 Location map of SKL between Shinminamata station and Shinomuta station. Seismic intensity contour map for **M**7.0 mainshock is overlaid (USGS 2019b)

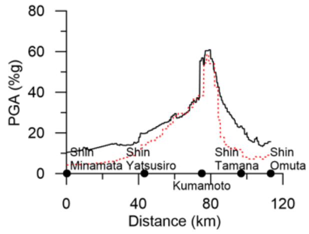

(a) Peak ground acceleration (%g)

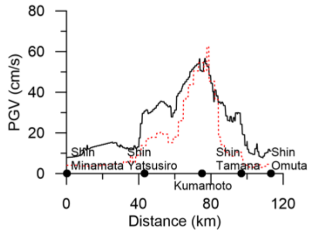

(b) Peak ground velocity (cm/s)

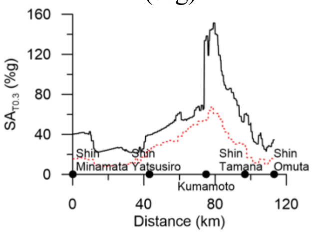

(c) Spectral acceleration at T=0.3 sec (%g)

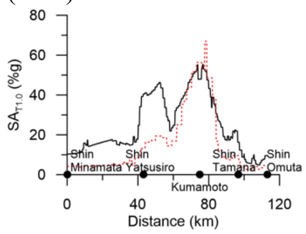

(d) Spectral acceleration at T=1.0 sec (%g)

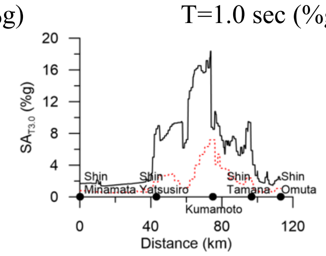

(e) Spectral acceleration at T=3.0 sec (%g)

Fig. 4 Intensity measures by the 2016 **M**6.2 foreshock (dotted red line) and **M**7.0 mainshock (solid black line) along the SKL

2.2.2 Damage distribution

We target the railway system between Shinminamata and Shinomuta stations which encompasses a sub-system between Shinyatsushiro and Shintamana stations damaged

Table 2 Damage description along the SKL written in the MLIT report (MLIT 2016)

Dist. (km)	Damage Description	Name of Location
43.2 – 75.0	33 cracks in the viaduct column	Shinyatsushiro to Kumamoto
75.0 – 96.8	122 fall-off of noise barrier walls	Kumamoto to Shintamana
75.0 – 96.8	4 damage on the viaduct bearings	Kumamoto to Shintamana

Table 3 Damage level and damage description from the SKL case history

DL	Damage State	Target structure type	Damage Description
2	Minor	Viaduct	- Crack in the viaduct column - Fall-off of noise barrier wall - Damage on the bearing

by the 2016 Kumamoto earthquakes. Collecting damage description resources, we found that there were slight and moderate damage on viaduct, but no damage on tunnel. We summarize one damage description resource, the MLIT report (MLIT 2016) in Table 2. As noted above, the damage location is not specified in detail so that we only know the total amount of damage within a region. Considering definition of damage levels used for the 2004 Niigata event (Table 1) and damage states from HAZUS model, we assigned only *DL*=2 to all damage states shown in Table 2. *DL* and the associated damage descriptions are summarized in Table 3. As a result, total 25 segments in SKL were damaged with *DL*=2 by the Kumamoto earthquakes.

3. Seismic fragility curves

3.1 Methodology

We statistically aggregate seismic fragility curve using ground motion intensities and damage levels assigned from a specific event following the procedure suggested by Baker (2015). The fragility function, the probability of damage exceeding a certain damage level given an *IM*, can be denoted as follows (Porter *et al.* 2007):

$$F_{dl}(IM) = P(DL \geq dl | IM = im) \tag{1}$$

where *DL* is a damage level, *dl* is a target damage level, and *im* is a target *IM*. The $F_{dl}(IM)$ is the probability exceeding *dl* at a given *IM*, which is ranged from zero to unity. To predict $F_{dl}(IM)$, a cumulative distribution function (CDF) is often used as a functional form because it also ranges from zero to unity. We adopted a log-normal CDF as a functional form as follows:

$$F_{dl}(IM) = \Phi\left(\frac{\ln(IM) - \ln(x_m)}{\beta}\right) \tag{2}$$

where Φ indicates standard normal Gaussian CDF, x_m denotes median, and β is standard deviation in natural log unit of distribution. *IMs* are distributed log-normally so that many ground motion models use log-normal distribution for *IM* prediction (e.g., Boore *et al.* 2014).

Defining $F_{dl}(IM)$ in Eq. (2) needs to identify x_m and β. Baker (2015) uses maximum likelihood estimation (MLE) method to find x_m and β from data points. Kwak *et al.* (2016) also used MLE to fit fragility functions to seismic levee damage probability. In MLE, a likelihood of damage probability can be calculated as follows:

$$Likelihood = \prod_{j=1}^{m} \binom{n_j}{z_j} p_j^{z_j} (1 - p_j)^{n_j - z_j} \tag{3}$$

where *m* is the number of *IM* levels, n_j and z_j are the total number of segments and number of damaged segments subjected to the j^{th} *IM* level, respectively, and p_j is the probability exceeding a certain *dl* with j^{th} *IM* from Eq. (2). From Eq. (3), we can find x_m and β maximizing the log of the likelihood as Eq. (4). We use this method to find x_m and β toward best-fitted fragility curve to damage probabilities conditional on *IM*.

3.2 Empirical fragility curves for railway structure

Two metrics used for the fragility function in Eq. (2), x_m and β, contain important information for damage probability prediction. The median, x_m indicates an *IM* for which 50% probability of damage is expected. However, if empirical data is used for fragility function generation, x_m tends to be unrealistically high because generally no data points are available at high probability range (> 20%). The log-normal fit is regressed only using low probability data points. Hence, the x_m should be interpreted as a metric for a fit, not a meaningful value that indicates 50% probability of damage if it is obtained from regression analysis and data are only available at low probability range. The β indicates how the probability distribution is scattered. Narrow distribution (i.e., small β) provides more precise information for predicting the damage occurrence given a certain *IM*. On the other hand, wider distribution (i.e., large β) does not help much because the probability of damage gradually increases with *IM* in wide range.

If regression is performed to empirical data, the x_m is often very high and β is often wide. It is because the line is fitted to scattered data points. Also, regression to data points without any constraint is sometimes problematic because the higher damage level could have the higher damage probability than the lower damage level at a certain *IM*. For bridge and tunnel, HAZUS fixes β = 0.6 for fragility curve with ground shaking demand. To compare with HAZUS result and prevent probability reversal, we also fix the β within one *IM* type and find x_m with varying *DL* threshold.

$$MLE(x_m, \beta) = \max \prod_{j=1}^{m} \ln\binom{n_j}{z_j} + z_j \times \ln \Phi\left(\frac{\ln(IM_j) - \ln(x_m)}{\beta}\right) + (n_j - z_j) \times \ln\left(1 - \Phi\left(\frac{\ln(IM_j) - \ln(x_m)}{\beta}\right)\right) \tag{4}$$

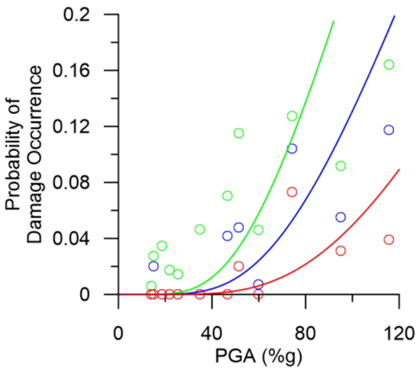

(a) Peak ground acceleration (%g)

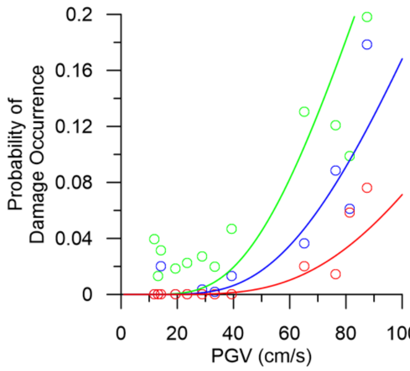

(b) Peak ground velocity (cm/s)

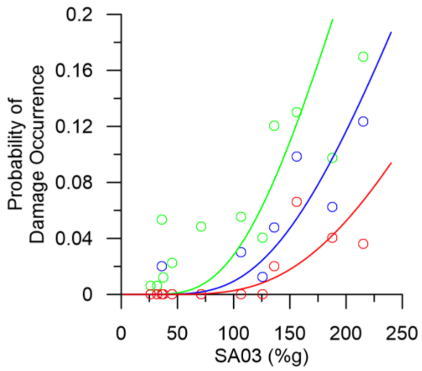

(c) Spectral acceleration at T=0.3 sec (%g)

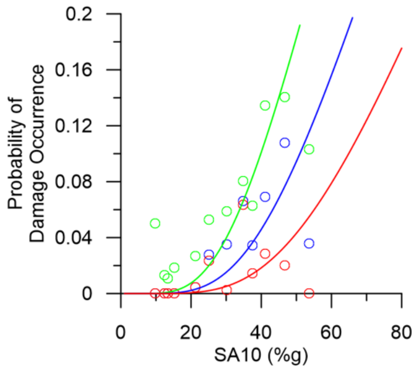

(d) Spectral acceleration at T=1.0 sec (%g)

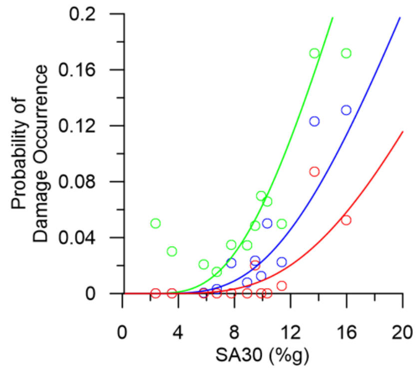

(e) Spectral acceleration at T=3.0 sec (%g)

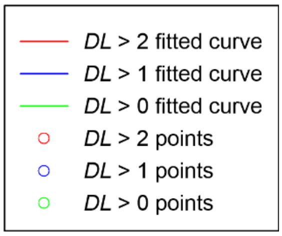

Fig. 5 Fragility curves regressed with β constraint including all structure type using the 2004 Niigata case history

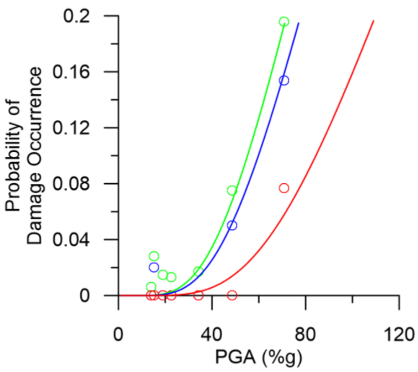

(a) Peak ground acceleration (%g)

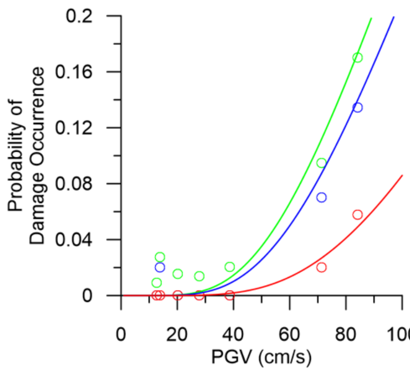

(b) Peak ground velocity (cm/s)

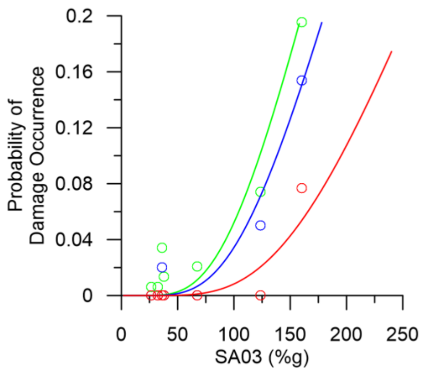

(c) Spectral acceleration at T=0.3 sec (%g)

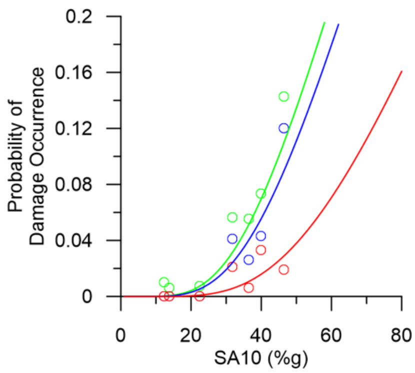

(d) Spectral acceleration at T=1.0 sec (%g)

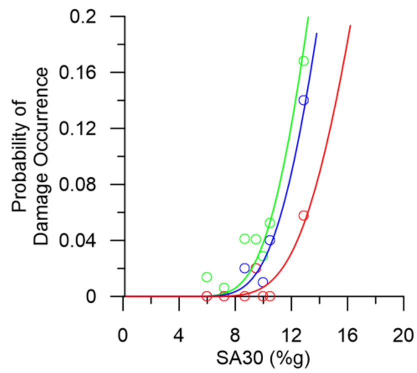

(e) Spectral acceleration at T=3.0 sec (%g)

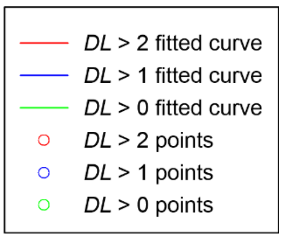

Fig. 6 Fragility curves regressed with β constraint for viaduct type using the 2004 Niigata case history

Table 4 Metrics for fragility curves depending on structure type and damage level. MLE indicates maximized log-likelihood estimate used for regression

Type	IMs	Metrics	DL > 0	DL > 1	DL > 2	Type	IMs	Metrics	DL > 0	DL > 1	DL > 2
All	PGA	x_m (%g)	154	129	182	Viaduct	PGA	x_m (%g)	119	129	182
		β	0.6	0.6	0.6			β	0.6	0.6	0.6
		MLE	-33.3	-22.7	-9.3			MLE	-8.8	-8.8	-2.6
	PGV	x_m (cm/s)	148	161	227		PGV	x_m (cm/s)	148	161	227
		β	0.6	0.6	0.6			β	0.6	0.6	0.6
		MLE	-17.4	-15.1	-5.6			MLE	-11.3	-10.9	-2.6
	$SA_{T0.3}$	x_m (%g)	265	298	421		$SA_{T0.3}$	x_m (%g)	265	298	421
		β	0.6	0.6	0.6			β	0.6	0.6	0.6
		MLE	-31.1	-16.0	-7.5			MLE	-9.0	-8.5	-3.0
	$SA_{T1.0}$	x_m (%g)	97	104	145		$SA_{T1.0}$	x_m (%g)	97	104	145
		β	0.45	0.6	0.6			β	0.45	0.6	0.6
		MLE	-25.7	-12.9	-12.3			MLE	-6.6	-6.5	-4.2
	$SA_{T3.0}$	x_m (%g)	17	18	21		$SA_{T3.0}$	x_m (%g)	17	18	21
		β	0.3	0.3	0.3			β	0.3	0.3	0.3
		MLE	-31.9	-11.3	-7.8			MLE	-8.4	-6.8	-4.2

For the probability assessment with a given *IM* and the development of the fragility function, we use the following procedure.

1. Sort segments based on *IM* value.
2. Bin segments with equal number. We selected 50 segments as a bin size.
3. Count damage occurrence within a bin.
4. Calculate probability of damage occurrence by dividing the number of damaged segments from (3) as a bin size from (2).
5. Fit a log-normal CDF function to data points obtained from (4) using the MLE method (Eq. 4) constraining β as a constant for one *IM* type.

We repeated the above procedure for each damage threshold (i.e., *DL*>0, *DL*>1, *DL*>2). The *DL*>3 is excluded because the number of damaged segments with *DL*=4 is very limited. In this study, five types of *IMs* (i.e., PGA, PGV, $SA_{T0.3}$, $SA_{T1.0}$, and $SA_{T3.0}$) were selected for seismic demand type.

We only developed fragility function for all structure type and viaduct type only. Tunnel is excluded because the damage probability data points are poorly scattered for this type so that fitting a fragility curve is not meaningful. Therefore, we suggest fragility curves with β constraint for all structure and viaduct. Fragility curves combining all structure without β constraint are shown in Yang and Kwak (2019).

Fig. 5 shows probability exceeding a certain damage level and fitted fragility curves for all structure including viaduct, tunnel, and station, and Fig. 6 shows for viaduct only. From the resulting fragility curves, we found that:

1. Viaduct fragility curve has more prediction power than all structure: low β and less scatter of data points. This may be caused because tunnel is located underground so that the *IM*s on the surface that used in this study would not be the true *IMs* for tunnel. This may induce data scatter for all structure type.
2. Among five *IM*s considered, $SA_{T3.0}$ provides the best-fitted fragility curve and the smallest β which gives sharp increase of probability. Although we used β = 0.6 to be the same β used in HAZUS in general, we selected β = 0.3 for viaduct case with $SA_{T3.0}$ (Fig. 6e). The β = 0.3 fits better than β = 0.6 to the data points for this case.
3. For viaduct, fragility curves for *DL* > 0 and 1 are very similar. It may be caused that the *DL* > 0 for viaduct are observed at low *IM*s where damage locations are very uncertain, which is ignored when regress fragility curve with β constraint.

4. Results and discussion

4.1 Validation with the 2016 Kumamoto event

To validate the fragility curve developed, we compare the probability of damage calculated from the developed fragility curve and the observed damage probability from the 2016 Kumamoto earthquake case history. We choose $SA_{T3.0}$ as a seismic demand because it predicts the damage with the least uncertainty as described in Section 3.2.

We first evaluated the total number of damaged segments by the 2016 mainshock within target SKL. We excluded the foreshock case because it is not clear that which event caused damage at specific locations. Since the mainshock generated greater *IM*s than the foreshock as shown in Fig. 4, we assumed that the majority of damage was occurred due to the mainshock.

We assigned only *DL*=2 to SKL based on the damage description (Table 3). The number of damaged segments with *DL*=2 is 25, and there is no tunnel damage. Hence, we use the fragility curve for x_m = 18 %g and β = 0.3 which is the case for [*DL* > 1, $SA_{T3.0}$, viaduct structure type) (Fig.

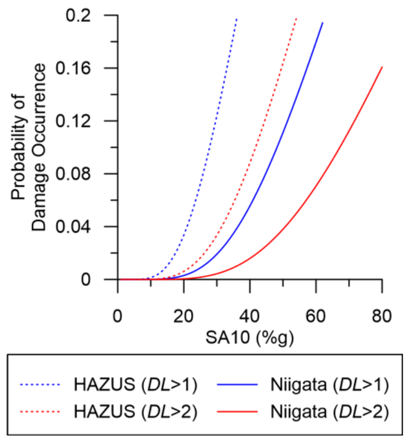

Fig. 7 Comparison of fragility curves of viaduct structure depending on damage levels between HAZUS and models developed in this study (Niigata)

6(e)). Ground motion observed along the SKL (Fig. 4(e)) is used for damage probability calculation at the target system. As a result, the sum of the damage probability is 22.21 which is very close to the total damaged segments by the 2016 event. It proves that the developed fragility curve predicts the total damage occurrence reasonably well even to another case history.

4.2 Comparison to HAZUS fragility curves

For a railway system, HAZUS provides fragility curves for track and roadbeds, railway bridges, railway tunnels, and railway system facilities (FEMA 2014). Herein we focus on the railway bridge case for comparison with empirically developed fragility curve (hereafter called Niigata) in this study. Since HAZUS uses $SA_{T1.0}$ and permanent ground deformation for seismic demands of fragility curves, we compare $SA_{T1.0}$ only. There are four damage states (DS) defined in HAZUS. Comparing to the *DL* description defined (Table 1), DS=1 is comparable to *DL*=2, and DS=2 is comparable to *DL*=3. Hence, target cases for comparison are $DL > 1$ and $DL > 2$.

Fig. 7 shows Niigata and HAZUS. The railway bridge type selected from HAZUS is HWB2 which is the type for the seismically designed major bridge (FEMA 2014). It can be seen that the HAZUS provides more conservative fragility curves than Niigata. For example, for $SA_{T1.0}$ = 30 %g, HAZUS predicts 12.4% of damage for $DL > 1$ and 3.4% for $DL > 2$, but Niigata predicts 1.9% for $DL > 1$ and 0.4% for $DL > 2$. We postulate that HAZUS models are based on relatively old damage functions (e.g., Basöz and Mander, 1999), which regards more vulnerable structures than modern structures resulting in more conservative fragility curves.

5. Conclusions

Seismic fragility curves for a high-speed railway system have been developed empirically. The 2004 **M**6.6 Niigata earthquake case history is used for the source of the model development, and the developed model is validated by comparing with another case history of the 2016 **M**7.0 Kumamoto earthquake. The developed fragility curves are also compared with existing fragility curves from HAZUS.

The target railway system is composed of generally three structure types: tunnel, viaduct, and station. The viaduct provides meaningful damage probability trend (i.e., probability increases with *IM*), but the damage probabilities for tunnel are poorly scattered. Hence, we only include viaduct for fragility curve development. The ground motion intensity that tunnel would get would be different with the one estimated in this study because tunnel is located underground. For station, the total number of segments is not enough to develop damage probability with robust manner.

We used five types of *IM*s: PGA, PGV, $SA_{T0.3}$, $SA_{T1.0}$, $SA_{T3.0}$ as seismic demands. Among those, $SA_{T3.0}$ gives the best-fitted model to data points and the smallest β which ensure that $SA_{T3.0}$ fragility model performs superior. We think that the long duration motion impacts the most to the damage of viaduct-type structure.

Applying [$SA_{T3.0}$, $DL > 1$, viaduct] fragility curve developed using the 2004 Niigata case history to the 2016 Kumamoto case history, we calculated the total sum of damage probability within the target railway system as 2221% (approximately 22 segments). The actual observed damaged segments are 25. It is promising that the developed fragility curve predicts reasonably well the total number of damaged segments from another case history. Comparing with HAZUS models, the developed fragility curves suggest lower probability of damage than the HAZUS given the same *IM*.

The fragility curve in this study is not developed from an in-depth research analyzing the damage mechanism for each infrastructure type; rather, the curve is developed statistically using a case history from a specific past event occurred in Japan. We validated the fragility model using another case history where both resulting damaged segments are in good agreement.

The fragility curve information provided herein could be used to assess preliminary expectation of seismic damage on high-speed railway system. However, we caution that another railway system in other regions or countries would have different construction standard or hazard mitigation effort, which would result in different fragility curve. For future study we are planning to perform numerical analysis of tunnel seismic behavior to fill the gap of fragility curve for railway infrastructure and further validate empirical viaduct fragility curve.

Acknowledgments

This research was supported by a grant (20CTAP-C152247-02) from Technology Advancement Research Program funded by Ministry of Land, Infrastructure and Transport of Korean government. We greatly appreciate the support. Also, we thank two anonymous reviewers and the associate editor for their constructive review comments.

References

Argyroudis, S.A. and Kaynia, A. (2015), "Analytical seismic fragility functions for highway and railway embankments and cuts", *Earthq. Eng. Struct. Dyn.*, **44**(11), 1863-1879. https://doi.org/10.1002/eqe.2563.

Argyroudis, S.A. and Pitilakis, K.D. (2012), "Seismic fragility curves of shallow tunnels in alluvial deposits", *Soil Dyn. Earthq. Eng.*, **35**, 1-12. https://doi.org/10.1016/j.soildyn.2011.11.004.

Baker, J.W. (2015), "Efficient analytical fragility function fitting using dynamic structural analysis", *Earthq. Spectra*, **31**(1), 579-599. https://doi.org/10.1193%2F021113EQS025M.

Balkaya, C. and Kalkan, E. (2004), "Seismic vulnerability, behavior and design of tunnel form building structures", *Eng. Struct.*, **26**(14), 2081-2099. https://doi.org/10.1016/j.engstruct.2004.07.005.

Basöz, N. and Mander, J. (1999), "Enhancement of the highway transportation lifeline module in HAZUS", *Nat. Inst. Build. Sci.*, **16**(1), 31-40.

Boore, D.M., Stewart, J.P., Seyhan, E. and Atkinson, G.M. (2014), "NGA-West2 equations for predicting PGA, PGV, and 5% damped PSA for shallow crustal earthquakes", *Earthq. Spectra*, **30**(3), 1057-1085. https://doi.org/10.1193%2F070113EQS184M.

da Porto, F., Tecchio, G., Zampieri, P., Modena, C. and Prota, A. (2016), "Simplified seismic assessment of railway masonry arch bridges by limit analysis", *Struct. Infra. Eng.*, **12**(5), 567-591. https://doi.org/10.1080/15732479.2015.1031141.

Federal Emergency Management Agency (FEMA) (2014), *HAZUS-MH 2.1 Technical Manual: Earthquake Model*.

Kim, H., Shin, C., Lee, T., Lee, J. and Park, D. (2014), "A study on the development of the seismic fragility functions of the high speed railway tunnels in use", *J. Kor. Geo-Environ. Soc.*, **15**(11), 67-75. https://doi.org/10.14481/jkges.2014.15.11.67.

Kircher, C.A., Whitman, R.V. and Holmes, W.T. (2006), "HAZUS earthquake loss estimation methods", *Nat. Haz. Rev.*, **7**(2), 45-59. https://doi.org/10.1061/(ASCE)1527-6988(2006)7:2(45).

Kwak, D.Y., Stewart, J.P., Brandenberg, S.J. and Mikami, A. (2016), "Characterization of seismic levee fragility using field performance data", *Earthq. Spectra*, **32**(1), 193-215. https://doi.org/10.1193%2F030414EQS035M.

Ministry of Land, Infrastructure, Transport and Tourism (MLIT) (2016), *Damage status of Shinkansen Kyushu Line by the Kumamoto Earthquake*, Supplement Material for the 13th meeting of Shinkansen Derailment Counter Measurement (in Japanese).

Li, L., Bu, Y., Jia, H., Zheng, S., Zhang, D. and Bi, K. (2017), "An improved approach for multiple support response spectral analysis of a long-span high-pier railway bridge", *Earthq. Struct.*, **13**(2), 193-200. https://doi.org/10.12989/eas.2017.13.2.193.

Liu, X.R., Li, D.L., Wang, J.B. and Wang, Z. (2015), "Surrounding rock pressure of shallow-buried bilateral bias tunnels under earthquake", *Geomech. Eng.*, **9**(4), 427-445. https://doi.org/10.12989/gae.2015.9.4.427.

Lu, J., Chen, X., Ding, M., Zhang, X., Liu, Z. and Yuan, H. (2019), "Experimental and numerical investigation of the seismic performance of railway piers with increasing longitudinal steel in plastic hinge area", *Earthq. Struct.*, **17**(6), 545-556. https://doi.org/10.12989/eas.2019.17.6.545.

Ogura, M. (2006), *The Niigata Chuetsu Earthquake - Railway Response and Reconstruction*, Japan Railway and Transport Review, 43/44.

Porter, K., Kennedy, R. and Bachman, R. (2007), "Creating fragility functions for performance-based earthquake engineering", *Earthq. Spectra*, **23**, 471-489. https://doi.org/10.1193%2F1.2720892.

Shao, G., Jiang, L. and Chouw, N. (2014), "Experimental investigations of the seismic performance of bridge piers with rounded rectangular cross-sections", *Earthq. Struct.*, **7**(4), 463-484. http://doi.org/10.12989/eas.2014.7.4.463.

United States Geological Survey (USGS) (2019a), *M 6.6 - near the West Coast of Honshu, Japan*. https://earthquake.usgs.gov/earthquakes/eventpage/usp000d6vk/executive.

United States Geological Survey (USGS) (2019b), *M 7.0 - 1km E of Kumamoto-shi, Japan*. https://earthquake.usgs.gov/earthquakes/eventpage/us20005iis/executive.

Yang, S. and Kwak, D. (2019), "Development of empirical fragility function for high-speed railway system using 2004 Niigata earthquake case history", *J. Kor. Geotech. Soc.*, **35**(11), 111-119 (in Korean). https://doi.org/10.7843/kgs.2019.35.11.111.

Yilmaz, M.F., Caglayan, B.O. and Ozakgul, K. (2019), "Probabilistic seismic risk assessment of simply supported steel railway bridges", *Earthq. Struct.*, **17**(1), 91-99. https://doi.org/10.12989/eas.2019.17.1.091.

CC